ELSEVIER

Journal of Alloys and Compounds 401 (2005) 238–248

Journal of ALLOYS AND COMPOUNDS

www.elsevier.com/locate/jallcom

Neutron diffraction and reflectivity studies of Eu chalcogenide based superlattices

H. Kępa[a,*], C.F. Majkrzak[b], P. Sankowski[c], P. Kacman[c], T.M. Giebultowicz[d]

[a] *Institute of Experimental Physics, Warsaw University, ul. Hoża 69, 00-681 Warszawa, Poland*
[b] *National Institute of Standards and Technology, Center for Neutron Research, Gaithersburg, MD 20899, USA*
[c] *Institute of Physics, Polish Academy of Sciences, Al. Lotników 32/46, 02-668 Warsaw, Poland*
[d] *Physics Department, Oregon State University, Corvallis, OR 97331, USA*

Received 30 September 2004; received in revised form 4 January 2005; accepted 15 January 2005
Available online 17 May 2005

Abstract

Neutron diffraction and reflectivity experiments performed on a number of magnetic semiconductor superlattices (SL), in search for interlayer coupling, are presented. Antiferromagnetic (AFM) EuTe/PbTe SL's and ferromagnetic (FM) EuS-based multilayers, with narrow-gap semiconductor (PbS) as well as insulating (YbSe) diamagnetic spacers, were studied. Pronounced interlayer magnetic correlations have been revealed in EuTe/PbTe by neutron diffraction. In the FM multilayers it was proven by neutron diffraction and reflectivity experiments that consecutive EuS layers are antiferromagnetically coupled. The strength of the AFM IC in EuS-based systems, determined by neutron reflectivity measurements in applied magnetic fields, was compared with the predictions of a tight-binding model. The results of theoretical calculations have been found to be in good qualitative agreement with the experimental data. Finally, the in-plane anisotropy and the in-plane magnetic domain population were studied by polarized neutron reflectivity. It was established that the preferred orientation of domain magnetization in each system coincides with one of the two possible in-plane easy axes: namely, with [2 1 0] in EuS/PbS, and with [1 1 0] in EuS/YbSe.

PACS: 75.25.+z; 75.50.Pp; 68.65.Cd; 61.12.Ha; 61.12.Ld

Keywords: Magnetic neutron diffraction; Polarized neutron reflectivity; Superlattices; Magnetic semiconductors

1. Introduction

In the last 15 years magnetic multilayered systems and the giant magnetoresistance resulting from interlayer coupling have been receiving considerable interest in both applied and fundamental scientific research. Interlayer coupling (IC) in multilayers and superlattices (SL's) has been observed in a wide variety of structures composed of metallic ferromagnetic (FM) layers alternating with nonmagnetic metallic spacer layers [1,2], as well as nonmetallic ones [3,4]. Those observations stimulated extensive theoretical studies that have resulted in a number of different models for the mechanism of interlayer coupling such as the RKKY model, the free-electron model, and several others. The most complete theory unifying all previous approaches has been constructed by Bruno [5]. However, neither interlayer coupling in systems composed of two nonmetallic materials, nor mechanisms that might give rise to coupling between antiferromagnetic layers have been considered in these works.

Yet, neutron diffraction data for three different SL systems composed of AFM and nonmagnetic semiconducting materials, reported in the mid-nineties [6–10], revealed the existence of pronounced interlayer correlations between the AFM blocks. More recently, coupling between FM-semiconductor layers has been found in EuS/PbS and EuS/YbSe SL's [11,12]. In these all-semiconductor systems, the carrier concentration is far too low to support any significant RKKY

* Corresponding author. Tel.: +48 22 5532197; fax: +48 22 6294229.
E-mail address: henryk.kepa@fuw.edu.pl (H. Kępa).

0377-0257/$ – see front matter © 2005 Elsevier B.V. All rights reserved.
doi:10.1016/j.jallcom.2005.01.055

interactions; moreover, in the case of antiferromagnetic EuTe/PbTe, MnTe/ZnTe, and MnTe/CdTe SL's, the AFM layers do not carry a net magnetic moment. Thus, the two main ingredients which were believed to play a crucial role in interlayer coupling – mobile carriers and layer magnetization – are absent in these cases. These results have clearly demonstrated that the magnetic interlayer coupling is not restricted to structures containing FM metallic components.

In this paper we present a review of experimental neutron diffraction and reflectivity studies of Eu chalcogenide based all-semiconductor superlattices. In Section 2 we describe the systems investigated, the sample preparation methods, and the experimental neutron scattering techniques employed in our research. In Section 3, the results of neutron diffraction studies of EuTe/PbTe, a SL system with antiferromagnetic layers, are presented. Studies of two ferromagnetic systems, EuS/PbS and EuS/YbSe, are reviewed in Sections 4 and 5, the former section is focused on experimental observations of interlayer correlation effects and a theoretical model developed in the context of these studies, whereas the latter section describes polarized neutron reflectometry investigations of the domain structure and in-plane magnetic anisotropy in the EuS layers in the two systems.

2. Samples and experimental techniques

Bulk EuTe is a classical Heisenberg antiferromagnet with a Néel temperature $T_N = 9.6$ K [13]. It crystallizes in the NaCl structure with $a = 6.598$ Å, its magnetic structure is the Type II AFM ordering in which the spins are ferromagnetically arranged in (1 1 1)-type lattice planes, and the neighboring planes are coupled antiferromagnetically to one another [14].

Electrically, EuTe is a wide gap (~ 2.5 eV) semiconductor with the 4f levels situated about 2 eV below the conduction band edge [13]. The diamagnetic constituent, PbTe, is a narrow gap (~ 0.19 eV) semiconductor, which also crystallizes in the NaCl structure and has a bulk lattice constant of 6.462 Å. This yields a close lattice-match to EuTe, with a mismatch of only 2.1% in the lattice constants.

The EuTe/PbTe SL samples were grown by molecular beam epitaxy on (1 1 1) oriented BaF_2 substrates as described in detail in Ref. [15]. Different $[(EuTe)_m|(PbTe)_n]_N$ SL stacks with m (varying from 2 to 10) monolayers of EuTe alternating with n (from 5 to 30) monolayers of PbTe, were deposited on 1–3 μm PbTe buffer layers. The SL bilayer repetition number N ranged typically from 300 to 400. The electron concentration in the PbTe layers was $\sim 10^{17}$ cm^{-3}, i.e., many orders of magnitude lower than in metals, and the EuTe layers were semiinsulating.

EuS, PbS, and YbSe are semiconducting materials which also crystallize in the rocksalt structure. All of them are very well lattice-matched with a lattice constant mismatch of about 0.5%. EuS is a well-known nonmetallic (semiinsulating) Heisenberg ferromagnet ($T_C = 16.6$ K). PbS is a diamagnet with a narrow band gap ($E_g = 0.3$ eV); its carrier concentration is typically of the order of 10^{17} to 10^{18} cm^{-3}. YbSe is a wide gap semiconductor with an energy gap $E_g = 1.6$ eV, being semiinsulating at low temperatures. The multilayers were grown epitaxially on monocrystalline KCl (0 0 1) substrates covered with a several hundred angstroms thick PbS buffer layer. An electron beam was used for EuS evaporation, and standard resistive heating for PbS evaporation. The quality of the SL's was examined by X-ray and neutron diffraction. Detailed studies of the growth and magnetic properties of EuS/PbS multilayers with thick PbS spacers (magnetically decoupled case) have been reported in Ref. [16].

All neutron scattering experiments described in this review were performed at the NIST Center for Neutron Research. For diffraction studies of the EuTe/PbTe systems, BT-2 and BT-9 triple-axis spectrometers were used. The instruments were set to elastic diffraction mode, with a pyrolitic graphite (PG) monochromator and analyzer, and a 5 cm PG filter in the incident beam. In most measurements the wavelength used was $\lambda = 2.35$ Å and the angular collimation was 40 min of arc throughout. Additionally, a number of diffraction experiments were carried out on the NG-1 reflectometer operated at neutron wavelength $\lambda = 4.75$ Å. The latter instrument yielded high intensity, high resolution spectra with a negligible instrumental broadening of the SL diffraction lines.

Neutron reflectivity measurements on the FM systems EuS/PbS and EuS/YbSe were carried out on the NG-1 reflectometer using both unpolarized and polarized neutron beams. All the magnetic neutron scattering patterns reported here have been measured at 4.3 K.

3. Interlayer spin correlations in EuTe/PbTe superlattices

Magnetic neutron diffraction is a powerful experimental tool capable of revealing the interlayer spin correlations in the case of AFM/nonmagnetic multilayers. The principle of the method is illustrated in Fig. 1.

A single broad maximum produced by a multilayer structure indicates the lack of coherence between the waves scattered by successive layers, meaning that the spin alignments in these layers are not correlated. Such a pattern is observed for the specimens with the highest (20 or more monolayers) PbTe spacer thicknesses (d_{PbTe}). However, as d_{PbTe} decreases, the character of the AFM reflections dramatically changes. As exemplified in Fig. 2 for thinner PbTe layers, a distinct pattern of narrower satellite peaks then emerges at regular intervals ΔQ_z corresponding to the SL periodicity. This clearly indicates the formation of magnetic interlayer correlations across the PbTe spacers. For d_{PbTe} below ~ 60 Å these magnetic satellites become the dominant part of the spectrum, the smaller the separation between EuTe layers the sharper and better resolved the SL satellite peaks.

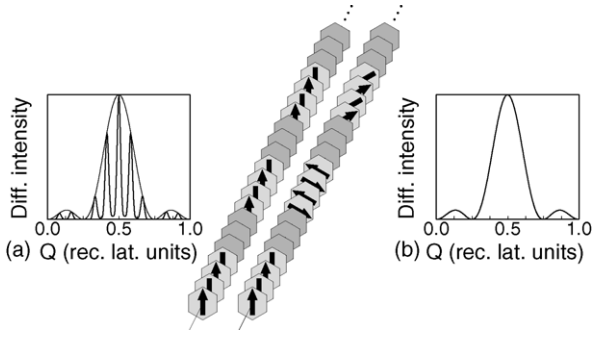

Fig. 1. Possible spin configurations in EuTe/PbTe SL's. (a) Correlated SL; monolayer magnetization directions in consecutive EuTe layers change in a regular fashion. Such an arrangement produces a diffraction pattern with a number of narrow fringes. (b) Uncorrelated SL; monolayer magnetization directions in consecutive EuTe layers change randomly, giving rise to a single broad neutron diffraction maximum.

To describe the observed shapes of the AFM diffraction patterns the possibility of partial correlations had to be considered. In order to describe such correlation in a quantitative manner, a parameter $p\,(|p| < 1)$ is introduced. Its definition is based on a somewhat simplified model of a SL with "Ising-type" AFM layers, i.e., one in which the spins comprising a given magnetic monolayer may take only an "up" or "down" orientation. If the layers in the SL structure are numbered $i = 1, 2, 3, \ldots, N$, then in any pair of of adjacent layers, $i, i+1$, the monolayer magnetization sequence may be either identical, or reversed corresponding, respectively to a "layer–layer correlation factor" of +1, or −1. The p parameter in the model is the mean value of these correlation factors for all $N-1$ layer pairs in the SL structure. As shown in the Appendix in Ref. [17], this model leads to the following expression for the magnetic diffraction intensity :

$$I(Q_z) \propto |F_{\mathrm{BL}}(Q_z)|^2 \frac{1-p^2}{1-2p\cos(Q_z D)+p^2} \qquad (1)$$

where D is the SL period and $|F_{\mathrm{BL}}(Q_z)|^2$ is the SL magnetic structure factor.

The results of the least-square fits of the Eq. (1) to the experimentally determined diffraction patterns, displayed in Fig. 2 by solid lines, show that the above equation describes the observed spectrum shapes very well indeed. The correlation parameter values obtained from the fits are also listed in each figure panel. As can be seen in Fig. 3 the decrease of the correlation parameter p with the nonmagnetic spacer thickness d_{PbTe} is approximately exponential. The solid line represents the fit of the exponential function to the points, some of them being scattered about the line, possibly due to the fluctuations of the PbTe layer thicknesses in the samples investigated.

In the case of AFM/nonmagnetic superlattices, the strength of the interlayer interactions giving rise to the interlayer spin correlations cannot be measured directly in neutron diffraction experiments. However, it is certainly a reasonable assumption that the behavior of the parameter p versus spacer thickness d_{PbTe} reflects the dependence of the interaction strength on d_{PbTe}. It should be noted that for FM/nonmagnetic SL's discussed in the next section, it is possible to directly determine the strength of the interlayer coupling by performing neutron scattering measurements in applied magnetic field.

4. Exchange interlayer coupling in ferromagnetic EuS/PbS and EuS/YbSe superlattices

The wide-angle diffraction techniques, which proved so successful in the studies of AFM/nonmagnetic SL's, can also be used for investigating FM/nonmagnetic SL's. However, in the latter case the measurements are much more challenging because of the proximity (in reciprocal space) of the magnetic SL scattering to the very strong Bragg scattering from the substrate and the buffer layer (in contrast, in antiferromagnets like EuTe, the magnetic Bragg scattering is located halfway between the structural diffraction maxima, so there is essentially no interference from the nuclear Bragg scattering from the substrate and that from the SL system itself). The measurements can be carried out in two different modes. One, in reflection geometry, is usually referred to as a 'longitudinal scan', and the other in transmission geometry, as a 'transverse scan' (see the diagram in Fig. 4).

Examples of diffraction patterns obtained in longitudinal scans are presented in Fig. 5(a) and (c) for two EuS/PbS SL's with different periodicity. In the scans performed above $T_{\mathrm{C}} = 18.5\,\mathrm{K}$, only a nuclear SL Bragg peak superimposed on the tail of the very strong KCl-substrate (0 0 2) reflection is seen. Below the Curie temperature the intensity on either side of the SL nuclear peak visibly increases due to additional magnetic scattering. The purely magnetic contribution to the diffracted intensity, obtained as a difference of the scans below and above T_{C}, is shown in Fig. 5(b) and (d). Only one magnetic SL peak is shown in the plots. The other one, located symmetrically with respect to the structural SL peak, disappears under the tail of the overwhelmingly stronger KCL (0 0 2) substrate peak.

The troublesome interference from the substrate reflection can be reduced by performing transverse scans as can be seen in Fig. 6. Here too, measurements below and above T_{C} were carried out to separate the magnetic contribution to the scattering. From the positions of the magnetic peaks in reciprocal space, it can be inferred that the magnetization vectors in the adjacent EuS layers are aligned in opposite directions, thus clearly pointing to AFM interlayer coupling in these SL's.

Neutron reflectometry appears to be a far superior tool for investigating the interlayer coupling in SL's composed of FM/nonmagnetic layers than the wide-angle diffraction method. Spontaneous magnetization of the FM layers contributes to the total neutron refraction index of the layer material and creates large optical contrast between magnetic and nonmagnetic layers, which in turn leads to a relatively high intensity of magnetically scattered neutrons. Moreover, the reflectivity data are collected only from the region of small

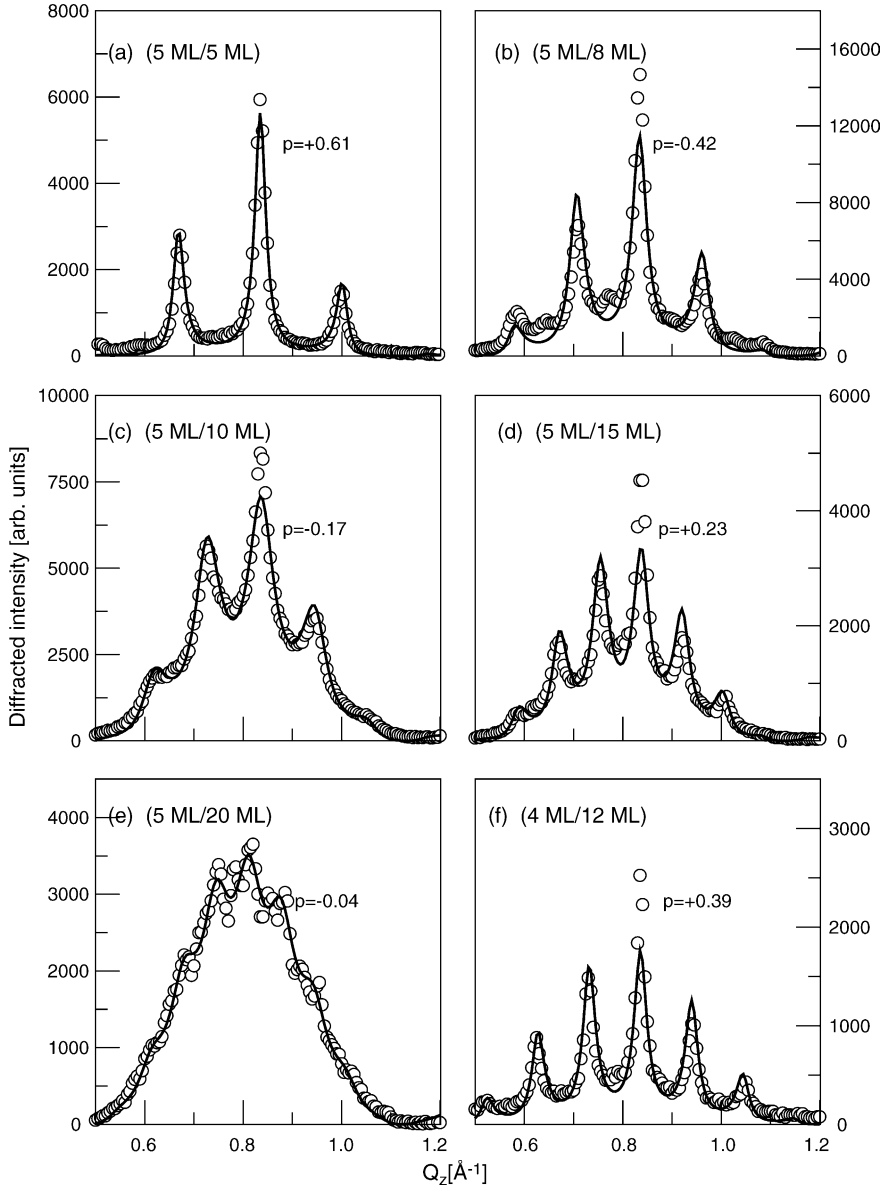

Fig. 2. Magnetic diffraction patterns from several EuTe/PbTe SL samples. The solid curves are fits of Eq. (1) to the data points. The fitted values of the partial correlation coefficient p for each pattern are shown in the figure.

Q-vectors where there are no interfering Bragg reflections from the crystal structure.

Fig. 7 shows typical reflectivity profiles obtained for EuS/PbS and EuS/YbSe samples. In zero applied magnetic field, pronounced peaks at the Q_z position corresponding to twice the chemical SL periodicity were observed in both systems. Again, these maxima are clear indication of the AFM alignment of the magnetizations in successive EuS layers. Measurements above and below the Curie temperature $T_C = 18.5 \pm 0.5$ K (22 and 4.3 K, respectively) were taken in order to distinguish the magnetic contribution from the structural part. Yet another way to confirm the magnetic origin of these peaks, is to take the reflectivity profile in an in-plane magnetic field. The application of a sufficiently strong, external magnetic field leads to completely parallel (saturated) alignment of the magnetization of EuS layers; thus the AFM peak disappears while the intensity of the FM peak at the structural position increases (see Fig. 7). As discussed below in closer detail, thorough investigation of the AFM peak behavior in a varying applied magnetic field can be used for extracting information about the strength of the interlayer coupling.

The results of the field dependence studies of the AFM peak in the neutron reflectivity profile are shown in Fig. 8 and in Fig. 9 for the EuS/PbS and EuS/YbSe samples, respectively. The measurement procedure starts with the samples in zero magnetic field. The field is gradually increased until the AFM peak disappears (saturation value), and then is decreased back to zero. In the next step the field direction is reversed and its magnitude is increased to the saturation value

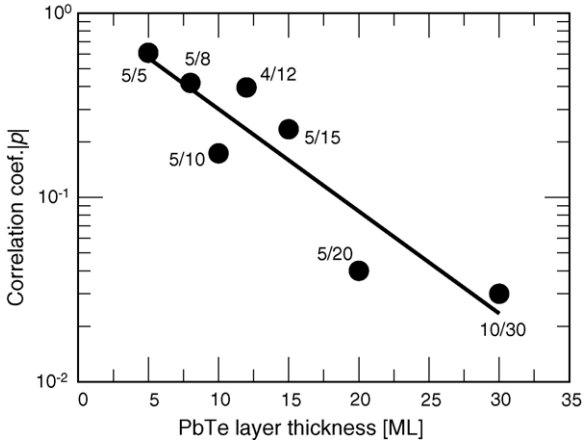

Fig. 3. The exponential dependence of the fitted values of the partial correlation coefficient p vs. PbTe spacer thickness.

and then again decreased to zero. This allows us to measure a sort of 'hysteresis loop' of the AFM coupled superlattice.

All the EuS/PbS and EuS/YbSe SL samples, cooled in zero-field through the transition temperature (T_C) show initially a strong AFM peak, indicating the existence of an efficient coupling mechanism.

The AFM peak for the EuS/PbS sample with the thinnest PbS spacer (4.5 Å) is recoverable. The removal of the external field leads to a nearly complete restoration of the AFM coupled state. The AFM peak of other EuS/PbS and EuS/YbSe samples is not recoverable. The samples remain in the ferro-

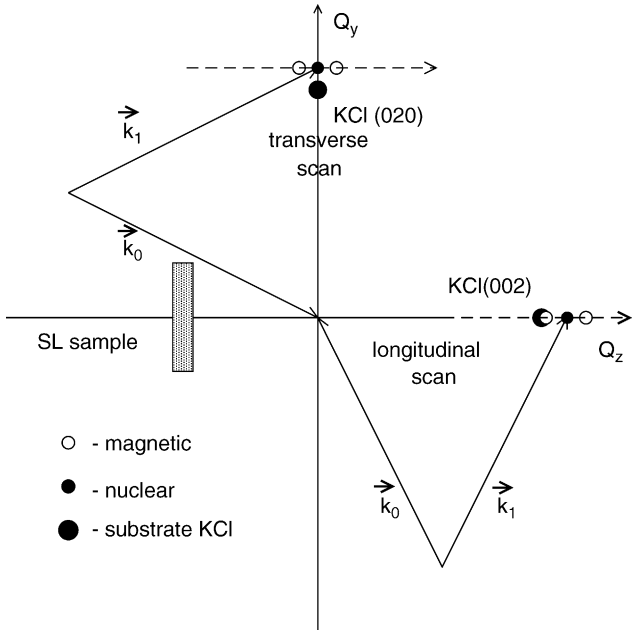

Fig. 4. Reciprocal lattice diagram showing possible scanning trajectories (transverse or longitudinal) that can be used in search for neutron diffraction maxima arising from interlayer spin correlations in FM superlattices. Also shown are (not to-scale) the positions of the corresponding nuclear and magnetic SL reciprocal lattice points as well as the substrate reflection points.

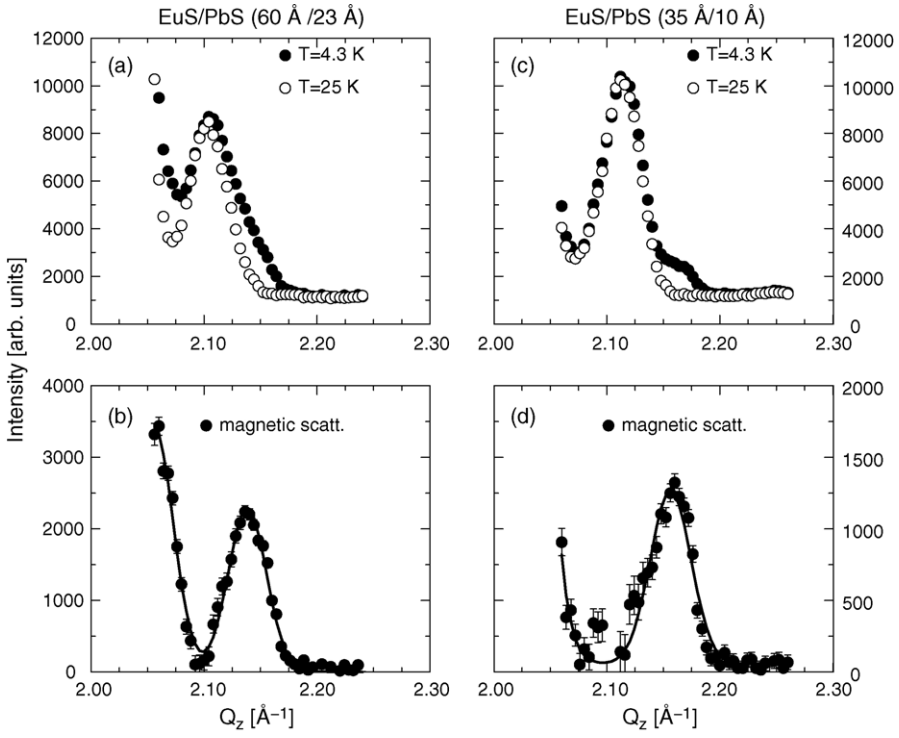

Fig. 5. (a) and (c) Neutron diffraction scans in reflection geometry (longitudinal scans) along the reciprocal lattice vector (0, 0, Q_z) for two EuS/PbS SL's taken below and above T_C. (b) and (d) Purely magnetic scattering spectrum obtained by performing a differential scan above and below the transition temperature for the same samples, respectively.

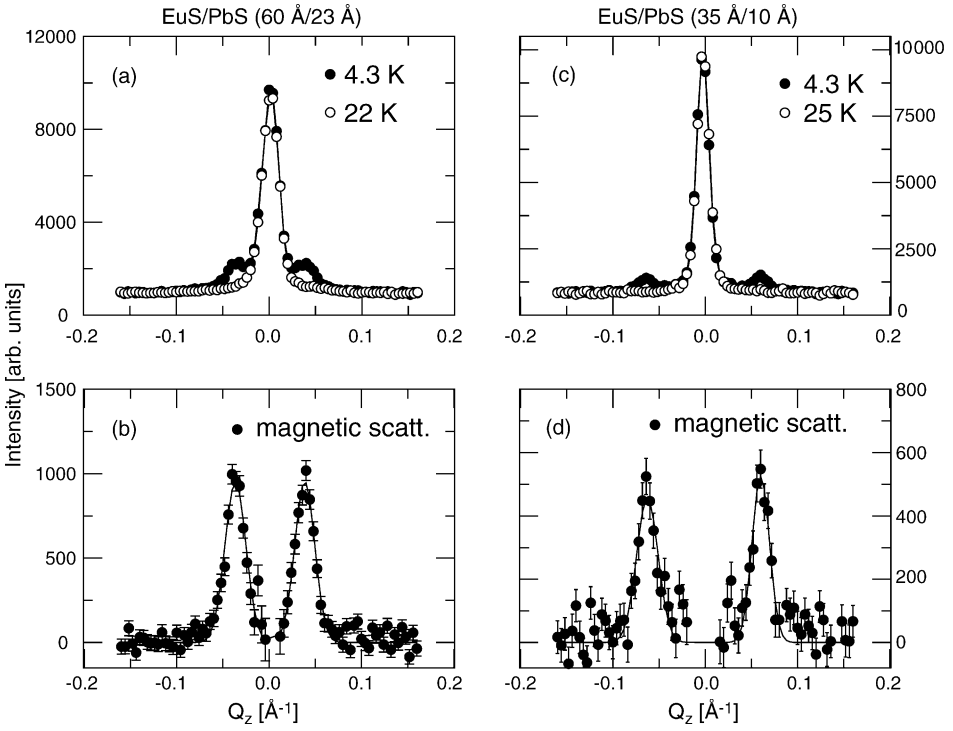

Fig. 6. (a) and (c) Neutron diffraction scans in transmission geometry (transverse scans) along the reciprocal lattice vector (0, 2.14, Q_z) for two EuS/PbS SL's taken below and above T_C. (b) and (d) The purely magnetic contribution to the scattering obtained as a difference of the scans below and above the transition temperature for the same samples, respectively.

magnetic configuration after the removal of the external field. Further application of the magnetic field in the opposite direction leads to the partial restoration of the intensity of the AFM peak. From the latter it can be inferred that the antiferromagnetic interlayer configuration could be recovered only in a fraction of the sample. How large this fraction is depends on the nonmagnetic spacer type (PbS or YbSe) and its thickness. Thus, for a sufficiently thin PbS spacer (∼ 10 Å, see Fig. 8b) one can observe a full restoration of the initial AFM state (in this particular example the fraction of the AFM coupled sample is even higher than it was in the initial zero-field-cooled state). The degree of this restoration diminishes with increase of the spacer thickness. In the case of YbSe, a wide-gap-semiconductor spacer, the degree of restoration is considerably lower than for a PbS layer of the same thickness (see Fig. 9). This suggests that the AFM coupling mechanism in the EuS/PbS samples is considerably stronger than in the EuS/YbSe samples with the same spacer thickness.

To analyze quantitatively the observed AFM hysteresis loops a modification of the Stoner–Wohlfarth model [18] has been employed. The total magnetic energy of the SL in the external magnetic field, consisting of the Zeeman energy term, the interlayer coupling energy term, and the anisotropy energy term, was minimized to obtain the magnetization vector sequence in successive EuS blocks. This minimum-energy sequence was further used to calculate the magnetic structure factors and, thus, the intensity of the AFM peaks. The values of the IC and the anisotropy constants, J and K, were obtained by least-square fitting of the calculated peak intensities for different magnetic fields to the experimental data. Details of the procedure are published elsewhere [19]. In Figs. 8 and 9 the fitted AFM hysteresis curves are presented by solid lines. The values of J for EuS/PbS SL's obtained from the fits are plotted versus the PbS layer thickness in Fig. 10 with open symbols.

To explain the origin of the IC in systems without conducting electrons, a model in which the exchange interactions are mediated by valence band electrons has been proposed [20–22]. The model does not assume any particular interaction mechanism, but attributes the IC to the sensitivity of the SL electronic energies to the magnetic order in the magnetic layers, i.e., accounts globally for the spin dependent band structure effects.

In [22] it was shown that the strength of the coupling in both EuS/PbS and EuS/YbSe SL's decreases exponentially with the nonmagnetic layer thickness (see Fig. 11). We would like to stress the following important fact emerging from the model. As can be seen in Fig. 11, for EuS layers separated by YbSe, the decrease of the calculated IC with the spacer thickness is considerably faster than for EuS layers separated by PbS. In other words, the model predicts weaker and shorter range interactions in EuS/YbSe multilayers than in the EuS/PbS ones.

The above model results are in good qualitative agreement with the observations which indeed indicate weaker and shorter range IC in the EuS/YbSe SL's than in the EuS/PbS

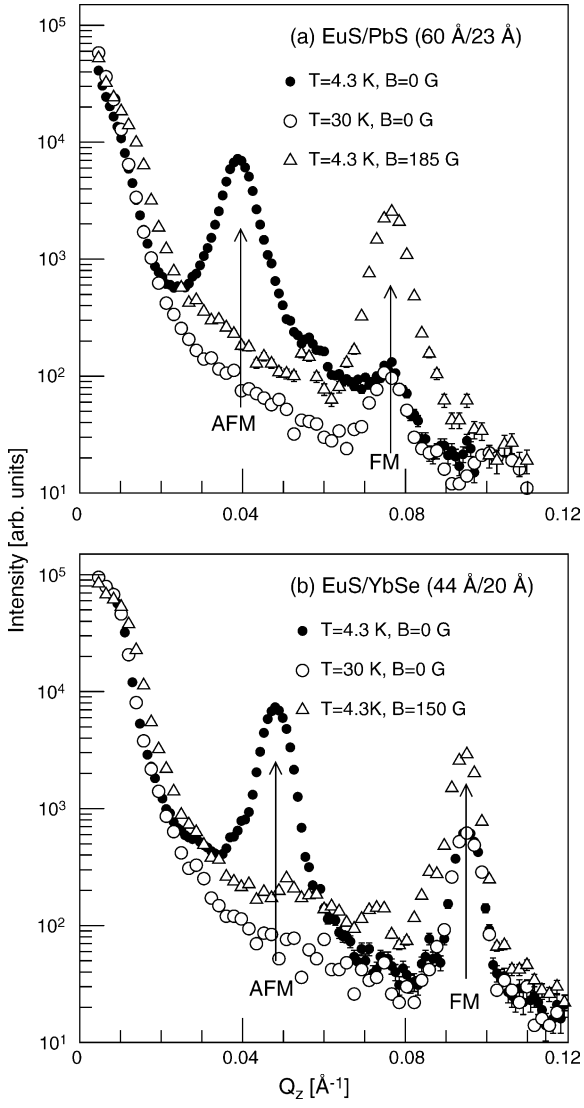

Fig. 7. Neutron reflectivity spectra for EuS/PbS (60 Å/23 Å) and EuS/YbSe (44 Å/20 Å) SL's, measured below and above T_C in zero (filled and empty circles, respectively) and in the saturating (triangles) magnetic fields.

ones. A quantitative comparison of the J values extracted from the neutron reflectivity experiments on EuS/PbS SL's with the model results is presented in Fig. 10. For up to $d_{PbS} \approx 25$ Å, the experimental J values are lower than those obtained from calculations. Within the experimental uncertainty, the data are consistent with the exponential decrease. However, the decay is slower than predicted. For thicker PbS layers the dependence of J with d_{PbS} visibly flattens out, showing that the IC is of longer range than predicted by the model. The observed behavior of J clearly suggest that there are two interaction components, one that decays exponentially with increasing spacer thickness, and another component that is approximately constant. Such a behavior is indicative for IC arising from dipolar interactions between EuS layers. Introducing those interactions into the overall picture may offer an explanation of some discrepancies between the measurements and model calculations.

If the magnetic layers in a SL system exhibit a domain structure with small enough average domain size (1 μm or less), the dipolar coupling, proposed in [23] for metallic structures, may become quite sizable. A characteristic feature of the dipolar coupling is a relatively weak dependence of its strength on the spacer thickness, as it follows from formula (9) in Ref. [23]. On the other hand, its strength depends critically on the lateral dimensions of the domains. As yet, there is no available information on this subject, so accurate calculations of the dipolar contribution to the IC in EuS-based superlattices cannot be carried out. Assuming that all the IC for spacer layers thicker than $\sim$ 25 Å are of dipolar origin, one can calculate its strength for thinner spacers (see the dashed line in Fig. 10) and thus subtract its contribution from the observed IC. The filled symbols in Fig. 10 represent the IC strength corrected in such a manner for dipolar effects. Now, the slope of the experimental dependence closely follows the slope of the theoretical curve, but still the experimental J values are almost an order of magnitude lower than the theoretical ones. The latter fact can possibly be attributed to the weakening of IC in real SL's due to the interfacial roughness, the theoretical calculations being performed for mathematically ideal multilayers.

Analogous reflectivity measurements in magnetic fields carried out for the EuS/YbSe SL's lead to the conclusion that, in the investigated range of YbSe spacer thickness (< 20 Å), all the observed IC is of dipolar origin. This is consistent with the theoretical expectations of much weaker valence band effects in EuS/YbSe, so that the dipolar interlayer interactions could prevail in these SL's.

The above theoretical model was also applied [21] to explain the interlayer spin correlations in the AFM EuTe/PbTe SL's discussed in Section 3. Again, the IC strength versus PbTe spacer thickness was found to follow an exponential decrease. As noted, it was not possible to experimentally measure the IC strength in these AFM SL's, but the exponential decay is clearly consistent with the behavior of the correlation parameter p in samples with various PbTe spacer thickness (see Fig. 3).

5. Polarized neutron reflectometry and in-plane anisotropy in EuS/PbS and EuS/YbSe superlattices

Specular [24] and off-specular [25] polarized neutron reflectometry (PNR) has recently been used to obtain closer insight into the lateral magnetic structure in thin films and SL's. Here, we review specular PNR studies that provide information about the in-plane magnetic anisotropy in the EuS layers in EuS/PbS and EuS/YbSe SL's and reveal some intriguing effects.

The principles of neutron polarization analysis, laid out in [26], are summarized in Fig. 12. In most neutron polarization analysis experiments four cross sections are measured, i.e., $(++)$, $(--)$, $(+-)$, and $(-+)$. In the first two the spin state of the neutron does not change (nonspin-flip or NSF processes)

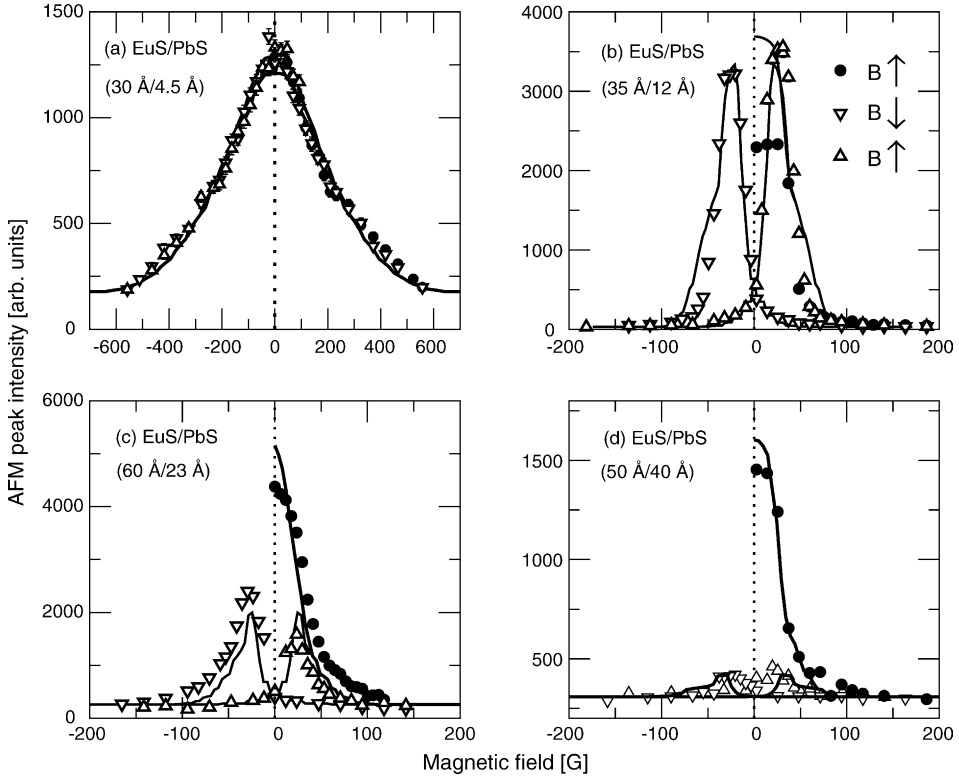

Fig. 8. The intensity of the AFM SL Bragg peak vs. magnetic field for four different EuS/PbS SL's. The lines represent the fitting of the Stoner–Wohlfarth model.

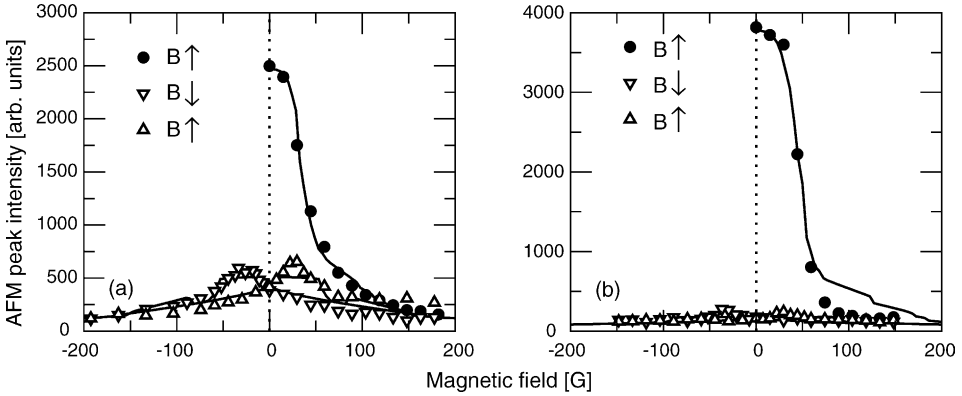

Fig. 9. The intensity of the AFM superlattice Bragg peak for two different EuS/YbSe SL's. The lines represent the Stoner–Wohlfarth model fitting.

whereas in the last two the neutron spin is reversed (spin-flip or SF processes).

Typical polarized neutron reflectivity spectra from the systems investigated are displayed in Fig. 13. The structural SL Bragg maximum (purely nuclear) is seen only in the NSF modes showing no splitting between (++) and (−−) cross-sections. A purely magnetic "half-order" maximum, arising from AFM interlayer coupling, shows a pronounced asymmetry in the NSF and SF intensities. This clearly indicates that the in-plane domain states allowed by the four-fold crystallographic symmetry of the (0 0 1)EuS epitaxial layers are not uniformly populated.

In order to investigate the distribution of in-plane magnetization directions of magnetic domains, and their relative population, the sample has to be mounted with a specific crystallographic axis pointing in a given (horizontal or vertical) direction. Then, a series of measurements have to be carried out with the sample rotated about the normal to its reflecting surface, thus changing the parallel and perpendicular components of the sample magnetization with respect to the neutron polarization direction.

The first series of such experiments was performed on EuS/PbS SL sample with 4.5 Å thick PbS spacer. This sample was found to exhibit the strongest interlayer coupling ever observed in any EuS/PbS SL. The sample was mounted with

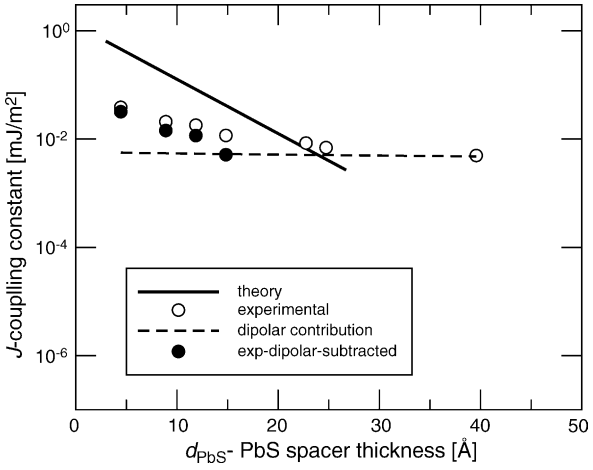

Fig. 10. The strength of the IC in the EuS/PbS superlattices vs. PbS spacer thickness. The open symbols represent the mean values of J obtained from the Stoner–Wohlfarth model fitting to the experiment. The solid line shows the theoretical predictions based on the tight-binding model calculations. The broken line represents the estimated dipolar contribution to the IC coupling. The experimental J values corrected for the dipolar contributions are shown as the filled symbols.

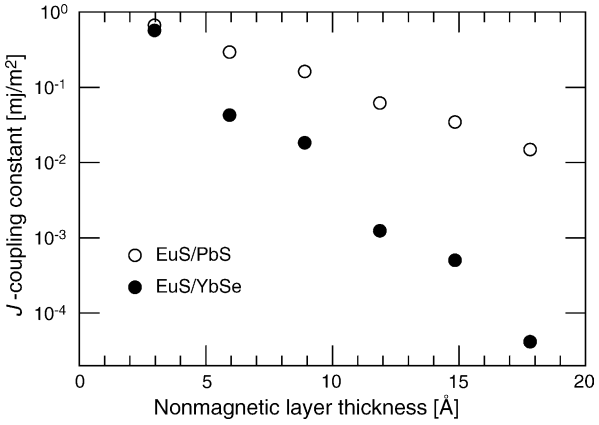

Fig. 11. Calculated interlayer coupling constants as a function of the spacer thickness for EuS/PbS and EuS/YbSe SL's.

the [2 1 0] axis in horizontal position. A series of measurements was then carried out with the sample rotated about the normal to its reflecting surface by $\pm 20^\circ$ from this position. The results are presented in Fig. 14(a).

Analogous data obtained for a EuS/YbSe superlattice mounted with the [1 0 0] in-plane axis vertical are shown in Fig. 14(b). For this orientation, all four polarized neutron reflectivities R^{++}, R^{-+}, R^{+-}, and R^{--} are of nearly equal intensity (see the panel marked $\Delta\phi = 0$ in Fig. 14(b)). Thus, for this sample the [1 1 0] and [1 $\bar{1}$ 0] in-plane directions are the easy axes along which the magnetization vectors are aligned.

To explain the observed effects it was assumed that the samples consist of two types of domains with their magnetizations aligned along two perpendicular directions, [1 1 0] and [1 $\bar{1}$ 0] in the case of the EuS/YbSe specimen, and [2 1 0] and [1 $\bar{2}$ 0] in the EuS/PbS sample. The area of the sample occupied by these domains is $S_1 = xS$ and $S_2 = (1 - x)S$, respectively, where the S is the total reflecting area of the

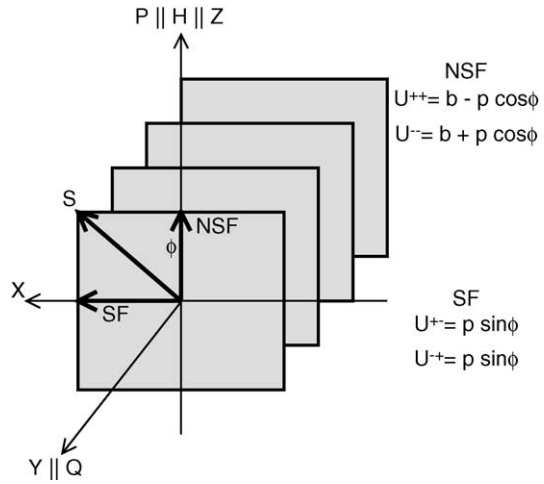

Fig. 12. The principles of the neutron polarization analysis. Neutron spin polarization vector **P** is along the Z direction, and so is the external magnetic field **H** (guide field). Vertical and horizontal atomic spin **S** (magnetization) components give rise to the nonspin-flip (NSF) and the spin-flip (SF) scattering, respectively. The SF scattering amplitudes U^{+-}/U^{-+} are purely magnetic, whereas in the NSF scattering (U^{++}/U^{--}) there is an interference of magnetic and nuclear terms. The + and − signs describe neutron spins 'up' and 'down', respectively; b and p denote neutron's nuclear and magnetic scattering amplitudes, respectively.

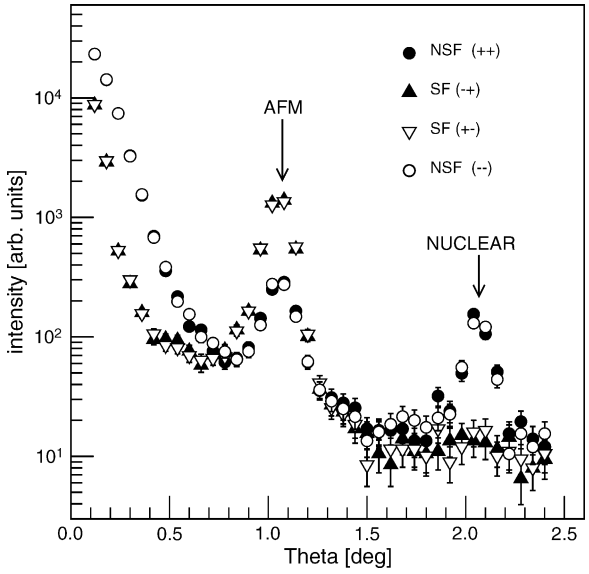

Fig. 13. Polarized neutron reflectivity profiles for a EuS/YbSe (46 Å/20 Å) SL with the in-plane [1 1 0] axis horizontal.

sample (see Fig. 15). It can be shown, that the ratio of NSF to SF intensities from such samples can be expressed in the following form:

$$\frac{I_{\mathrm{NSF}}}{I_{\mathrm{SF}}} = \frac{x\sin^2(\phi_0 + \Delta\phi) + (1-x)\cos^2(\phi_0 + \Delta\phi)}{x\cos^2(\phi_0 + \Delta\phi) + (1-x)\sin^2(\phi_0 + \Delta\phi)} \qquad (2)$$

where $\phi = \phi_0 + \Delta\phi$, ϕ_0 describes the initial sample alignment and $\Delta\phi$ is the angle of the sample rotation about the normal to the surface.

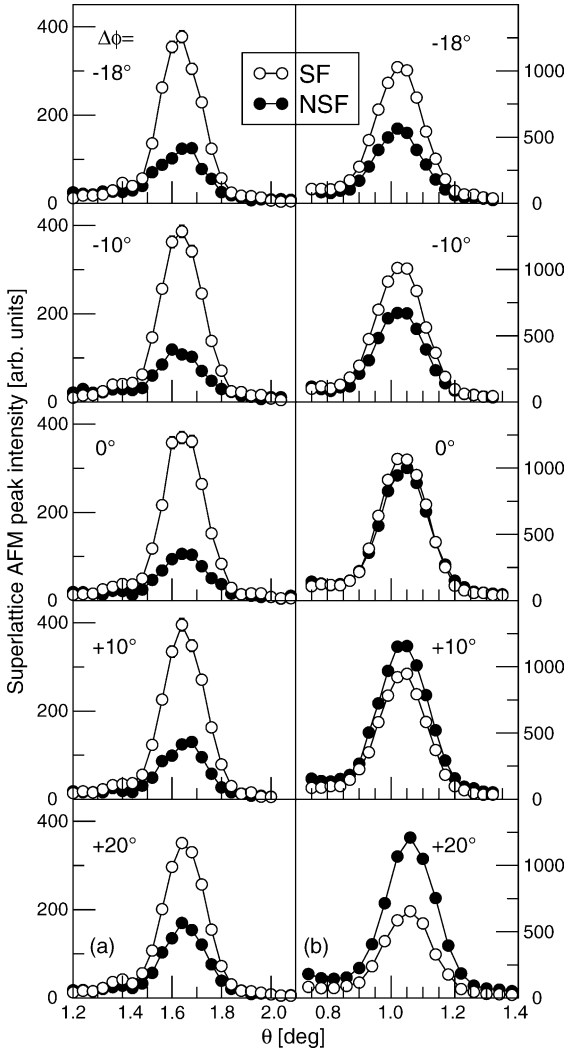

Fig. 14. The NSF and SF intensities of the AFM superlattice Bragg peaks for different sample orientations with respect to the neutron polarization direction: (a) EuS/PbS with [2 1 0] axis, and (b) EuS/YbSe with [0 1 0] axis in horizontal (when $\Delta\phi = 0$) positions.

The experimentally determined values of I_{NSF}/I_{SF} and the fit of Eq. (2) to the data points are presented in Fig. 16. The values of the x and ϕ_0 parameters obtained from the fits are also shown in Fig. 16 for both samples. The broken line shows the calculated ratio of NSF to SF intensities in the case of a uniaxial sample (for which $x = 1$) with the same alignments with respect to the polarization direction.

In bulk EuS crystal the easy axes lie along the [1 1 1]-type directions, whereas in the layered structures, due to the shape anisotropy, the magnetization directions are confined to the (0 0 1) growth plane of the layers. Due to the four-fold symmetry of the (0 0 1) layer one can expect analogous symmetry in the distribution of domain magnetization directions. The neutron reflectivity measurements performed in conjunction with rotating the samples about the axis normal to the reflecting surface essentially show the presence of a biaxial state with 90° domains. This would be in agreement with the crystallographic symmetry of the EuS layer, apart from the fact

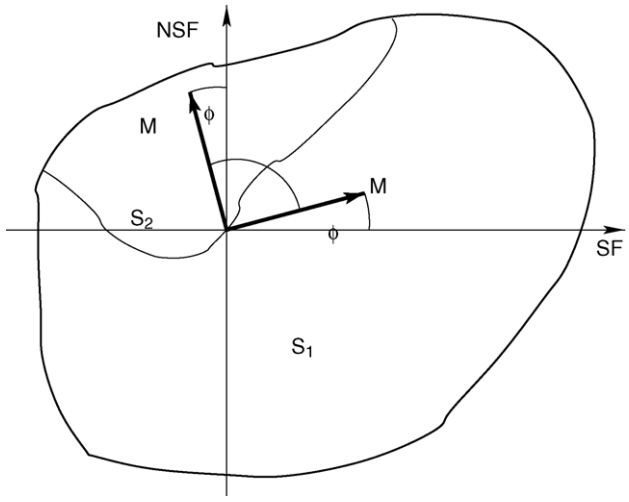

Fig. 15. A schematic view of the sample surface. The two areas labeled as S_1 and S_2 represent domains with magnetization vectors **M** along two perpendicular crystallographic axes.

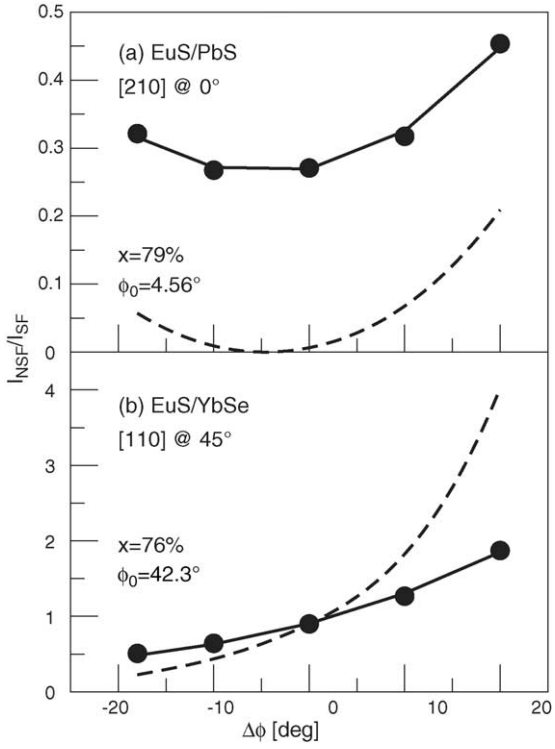

Fig. 16. NSF to SF intensity ratio as a function of the sample orientations with respect to the neutron polarization direction for two SL specimens of different composition. Solid lines represent the fits of Eq. (2) to the experimental data. Broken lines show NSF/SF ratios, calculated from Eq. (2), for uniaxial samples (i.e., for $x = 1$) with the same alignment. The fitted values of ϕ_0 reflect the actual initial sample misalignment.

that the populations of the two types of domains are far from being equal. In both investigated specimens, EuS/PbS and EuS/YbSe, more than three quarters of the magnetic material volume (76% and 79%, respectively) belongs to one type of domain. Thus, this result shows that the four-fold symmetry of the EuS layers is, if not broken, then at least "weakened"

as compared to the bulk crystal.

Moreover, it was found that the domain magnetizations in EuS/PbS and EuS/YbSe superlattices were aligned along different in-plane directions, the easy axes being ⟨2 1 0⟩ and ⟨1 1 0⟩, respectively.

The exact physical mechanism underlying the observed deviation from a perfect cubic symmetry is not yet clear. Apart from the shape anisotropy, a number of mechanisms may contribute in different ways to the resultant magnetic anisotropy in thin films. These might be anisotropic relaxation of strain induced by the lattice mismatch, nonisotropic steps on the substrate surface, or interfacial compound formation. However, the exact source of the uniaxial component in the present case of EuS-based SL's still remains an open issue.

6. Summary

In this review the role of neutron scattering techniques in the investigations of the magnetic structure of semiconductor multilayers has been presented. Neutron diffraction and reflectivity experiments, performed on a number of magnetic semiconductor superlattices, have shown that the phenomenon of interlayer exchange coupling is not restricted to the metallic multilayers composed of ferromagnetic/nonmagnetic transition metals only. In semiconductor systems, where the concentration of mobile carriers is many orders of magnitude lower than in metals, a new physical mechanism, different than RKKY, responsible for the IC had to be found. Such a mechanism, based on a valence band effects, has been developed and its conclusions concerning the type of the coupling, its strength and the range, compared with the results of neutron diffraction and reflectivity experiments. The results of theoretical calculations have been found to be in good qualitative agreement with the experimental data. Finally, the ability of the polarized neutron reflectometry of disclosing the in-plane anisotropy and the in-plane magnetic domain population has been discussed and illustrated with the results for semiconductor EuS/PbS and EuS/YbSe superlattices.

Acknowledgements

Work supported by NSF DMR-0204105, CRDF UP2-2444-KH-02, PBZ-KBN-044/P03/2001 grants, FENIKS (EC:G5RD-CT-2001-00535) and ERATO Semiconductor Spintronics projects.

References

[1] P. Grünberg, R. Schreiber, Y. Pang, M.B. Brodsky, H. Sowers, Phys. Rev. Lett. 57 (1986) 2442.
[2] S.S.P. Parkin, Phys. Rev. Lett. 67 (1991) 3598.
[3] S. Toscano, B. Briner, H. Hopster, M. Landolt, J. Magn. Magn. Mater. 114 (1992) L6.
[4] L. Briner, M. Landolt, Phys. Rev. Lett. 73 (1994) 340.
[5] P. Bruno, Phys. Rev. B 52 (1995) 411.
[6] T.M. Giebultowicz, V. Nunez, G. Springholz, G. Bauer, J. Chen, M.S. Dresselhaus, J.K. Furdyna, J. Magn. Magn. Mater. 140–144 (1995) 635.
[7] V. Nunez, T.M. Giebultowicz, W. Faschinger, G. Bauer, H. Sitter, J.K. Furdyna, J. Magn. Magn. Mater. 140–144 (1995) 633.
[8] J.J. Rhyne, J. Lin, J.K. Furdyna, T.M. Giebultowicz, J. Magn. Magn. Mater. 177–181 (1998) 1195.
[9] H. Kępa, K.I. Goldman, T.M. Giebultowicz, C.F. Majkrzak, G. Springholz, H. Krenn, S. Holl, F. Schinagl, G. Bauer, Physica E 2 (1998) 399.
[10] K.I. Goldman, G. Springholz, H. Kepa, T.M. Giebultowicz, C.F. Majkrzak, G. Bauer, Physica B 241–243 (1998) 710.
[11] H. Kępa, J. Kutner-Pielaszek, J. Blinowski, A. Twardowski, C.F. Majkrzak, T. Story, P. Kacman, R.R. Gałązka, K. Ha, H.J.M. Swagten, W.J.M. de Jonge, A.Y. Sipatov, V. Volobuev, T.M. Giebultowicz, Europhys. Lett. 56 (2001) 54.
[12] H. Kępa, P. Sankowski, P. Kacman, A.Y. Sipatov, C.F. Majkrzak, T.M. Giebultowicz, J. Magn. Magn. Mater. 272–276 (2004) 323.
[13] P. Wachter, in: K.A. Gschneider, L. Eyring (Eds.), Handbook on the Physics and Chemistry of Rare Earth, North Holland, Amsterdam, 1979. p. 507.
[14] G. Will, S.J. Pickart, H.A. Alperin, R. Nathans, J. Phys. Chem. Solids 24 (1963) 1679.
[15] G. Springholz, G. Bauer, Appl. Phys. Lett. 62 (1993) 2399.
[16] A. Stachow-Wójcik, T. Story, W. Dobrowolski, M. Arciszewska, R.R. Gałązka, M.W. Kreijveld, C.H.W. Swüste, H.J.M. Swagten, W.J.M. de Jonge, A. Twardowski, A.Y. Sipatov, Phys. Rev. B 60 (1999) 15220.
[17] H. Kępa, G. Springholz, T.M. Giebultowicz, K.I. Goldman, C.F. Majkrzak, P. Kacman, J. Blinowski, S. Holl, H. Krenn, G. Bauer, Phys. Rev. B 68 (2003) 024419.
[18] E.C. Stoner, E.P. Wohlfarth, Philos. Trans. R. Soc. London, Ser. A 240 (1948) 599.
[19] P. Sankowski, H. Kępa, P. Kacman, A.Y. Sipatov, C.F. Majkrzak, T.M. Giebultowicz, Acta Phys. Pol. A 105 (2004) 607.
[20] J. Blinowski, P. Kacman, Acta Phys. Pol. A 92 (1997) 719.
[21] J. Blinowski, P. Kacman, Phys. Rev. B 64 (2001) 045302.
[22] P. Sankowski, P. Kacman, Acta Phys. Pol. A 103 (2003) 621.
[23] J.A. Borchers, P.M. Gehring, R.W. Erwin, J.F. Ankner, C.F. Majkrzak, T.L. Hylton, K.R. Coffey, M.A. Parker, J.K. Howard, Phys. Rev. B 54 (1996) 9870.
[24] W.T. Lee, S.G.E. te Velthuis, G.P. Felcher, F. Klose, T. Gredig, E.D. Dahlberg, Phys Rev. B 65 (2002) 224417.
[25] S. Langridge, J. Schmalian, C.H. Marrows, D.T. Dekadjevi, B.J. Hickey, Phys. Rev. Lett. 85 (2000) 4964.
[26] R.M. Moon, T. Riste, W.C. Koehler, Phys. Rev. 181 (1969) 920.